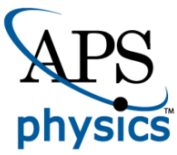

Evidence for BFKL and saturation dynamics from dihadron spectra at the LHC

Kevin Dusling and Raju Venugopalan

Phys. Rev. D **87**, 051502 — Published 11 March 2013

DOI: 10.1103/PhysRevD.87.051502

Evidence for BFKL and saturation dynamics from di-hadron spectra at the LHC

Kevin Dusling[1] and Raju Venugopalan[2]

[1] *Physics Department, North Carolina State University, Raleigh, NC 27695, USA*
[2] *Physics Department, Brookhaven National Laboratory, Upton, NY 11973, USA*

We demonstrate that rapidity separated di-hadron spectra in high multiplicity proton-proton collisions at the LHC can be quantitatively described by a combination of BFKL and saturation dynamics. Based on these results, we predict the systematics of di-hadron spectra in proton-nucleus collisions at the LHC.

Proton-proton collisions in the high energy Regge-Gribov asymptotics of QCD are described by the exchange of ladder like emissions of gluons. These gluons carry very small fractions x of the longitudinal momenta of the colliding protons but have fixed but sufficiently large transverse momenta such that the coupling α_S governing their emission is weak. In these high energy asymptotics, large logarithms of x accompany every such emission; multi-particle production is described by the Balitsky-Fadin-Kuraev-Lipatov (BFKL) equation [1, 2] which performs a resummation of $\alpha_S \ln(x)$ terms that appear at each rung of the QCD ladder. The BFKL bremsstrahlung evolution equation in x can be contrasted to the Dokshitzer-Gribov-Lipatov-Altarelli-Parisi (DGLAP) equations [3–5] corresponding to QCD evolution with squared momentum resolution Q^2.

An important feature of QCD in Regge-Gribov asymptotics is gluon saturation [6, 7], which predicts that gluons have a maximal phase space occupancy for transverse momenta below a saturation scale $Q_S(x)$ in hadron wavefunctions. $Q_S(x)$ is significantly larger at small x than the intrinsic QCD scale, making feasible a weak coupling Effective Field Theory (EFT) treatment of the non-perturbative dynamics of QCD saturation [8]. This Color Glass Condensate (CGC) EFT describes both the growth of gluon distributions via BFKL evolution and the onset of gluon saturation [9].

In this letter, we demonstrate that a combination of BFKL and saturation dynamics provides a good description of high multiplicity di-hadron spectra in proton-proton (p+p) collisions at the LHC. These spectra were measured by the CMS collaboration [10] in events with a high charged hadron multiplicity ($N > 110$) in the rapidity range of $2 \leq |\Delta\eta| \leq 4$. On the nearside (with azimuthal separations $\Delta\phi \approx 0$), the di-hadron spectra display a novel and mostly unanticipated collimation called the "ridge". We showed previously [11] that the di-hadron yield in the ridge is described by "Glasma graphs" [12–14] which are enhanced by gluon saturation in high multiplicity events relative to minimum bias by α_S^{-8}, a factor of 10^4–10^5 for typical values of the coupling α_S.

Emission on the awayside ($\Delta\phi \approx \pi$) is dominated by the better known "back-to-back" QCD graphs. Gluon emissions between the tagged partons are shown to be essential and described by a universal BFKL Green function. Both Glasma and BFKL graphs are illustrated in fig. 1. Detailed exploration of di-hadron spectra has the potential to uniquely pin down the underlying perturbative "QCD string" dynamics, gluon saturation, and the interplay between the two. Proton-Lead (p+Pb) collisions at the LHC at $\sqrt{s} = 5.02$ TeV provide valuable information in this regard; we therefore make predictions for di-hadron spectra in these collisions.

We first examine the Glasma Graphs for correlated two gluon production. The leading contributions in $\mathbf{p}_T/Q_S$ are expressed in terms of the two particle momentum space rapidities $y_{p,q}$ and transverse momenta $\mathbf{p}_T, \mathbf{q}_T$ as [11]

$$\frac{d^2N^{\text{corr.(1)}}_{\text{Glasma}}}{d^2\mathbf{p}_T d^2\mathbf{q}_T dy_p dy_q} = \frac{C_2}{\mathbf{p}_T^2\mathbf{q}_T^2}\int_{\mathbf{k}_T}(D_1 + D_2)\,, \tag{1}$$

with $C_2 = \frac{\alpha_S(\mathbf{p}_T)\,\alpha_S(\mathbf{q}_T)}{4\pi^{10}}\frac{N_C^2\,S_\perp}{(N_C^2-1)^3\,\zeta}K_{\text{Glasma}}$ and

$$\begin{aligned} D_1 &= \Phi^2_{A_1}(y_p,\mathbf{k}_T)\Phi_{A_2}(y_p,\mathbf{p}_T-\mathbf{k}_T)D_{A_2} \\ D_2 &= \Phi^2_{A_2}(y_q,\mathbf{k}_T)\Phi_{A_1}(y_p,\mathbf{p}_T-\mathbf{k}_T)D_{A_1}\,, \end{aligned} \tag{2}$$

where $D_{A_{2(1)}} = \Phi_{A_{2(1)}}(y_q,\mathbf{q}_T+\mathbf{k}_T) + \Phi_{A_{2(1)}}(y_q,\mathbf{q}_T-\mathbf{k}_T)$.

We extend our previous calculation by evaluating addition diagrams [12, 13] that are formally subleading in $\mathbf{p}_T/Q_S$ but are important for a quantitative analysis; their contribution is expressed as

$$\frac{d^2N^{\text{corr.(2)}}_{\text{Glasma}}}{d^2\mathbf{p}_T d^2\mathbf{q}_T dy_p dy_q} = \frac{C_2}{\mathbf{p}_T^2\mathbf{q}_T^2}\sum_{j=\pm}\left(A_1(\mathbf{p}_T,j\mathbf{q}_T) + \frac{1}{2}A_2(\mathbf{p}_T,j\mathbf{q}_T)\right)\,, \tag{3}$$

with[15] $A_1 = \delta^2(\mathbf{p}_T+\mathbf{q}_T)\left[\mathcal{I}_1^2+\mathcal{I}_2^2+2\mathcal{I}_3^2\right]$, such that

$$\begin{aligned} \mathcal{I}_1 &= \int_{\mathbf{k}_{1\perp}}\Phi_{A_1}(y_p,\mathbf{k}_{1\perp})\Phi_{A_2}(y_q,\mathbf{p}_T-\mathbf{k}_{1\perp})\frac{\left(\mathbf{k}_{1\perp}\cdot\mathbf{p}_T-\mathbf{k}_{1\perp}^2\right)^2}{\mathbf{k}_{1\perp}^2\left(\mathbf{p}_T-\mathbf{k}_{1\perp}\right)^2}\,, \\ \mathcal{I}_2 &= \int_{\mathbf{k}_{1\perp}}\Phi_{A_1}(y_p,\mathbf{k}_{1\perp})\Phi_{A_2}(y_q,\mathbf{p}_T-\mathbf{k}_{1\perp})\frac{|\mathbf{k}_{1\perp}\times\mathbf{p}_T|^2}{\mathbf{k}_{1\perp}^2\left(\mathbf{p}_T-\mathbf{k}_{1\perp}\right)^2}\,, \\ \mathcal{I}_3 &= \int_{\mathbf{k}_{1\perp}}\Phi_{A_1}(y_p,\mathbf{k}_{1\perp})\Phi_{A_2}(y_q,\mathbf{p}_T-\mathbf{k}_{1\perp})\frac{\left(\mathbf{k}_{1\perp}\cdot\mathbf{p}_T-\mathbf{k}_{1\perp}^2\right)|\mathbf{k}_{1\perp}\times\mathbf{p}_T|}{\mathbf{k}_{1\perp}^2\left(\mathbf{p}_T-\mathbf{k}_{1\perp}\right)^2}\,. \end{aligned}$$

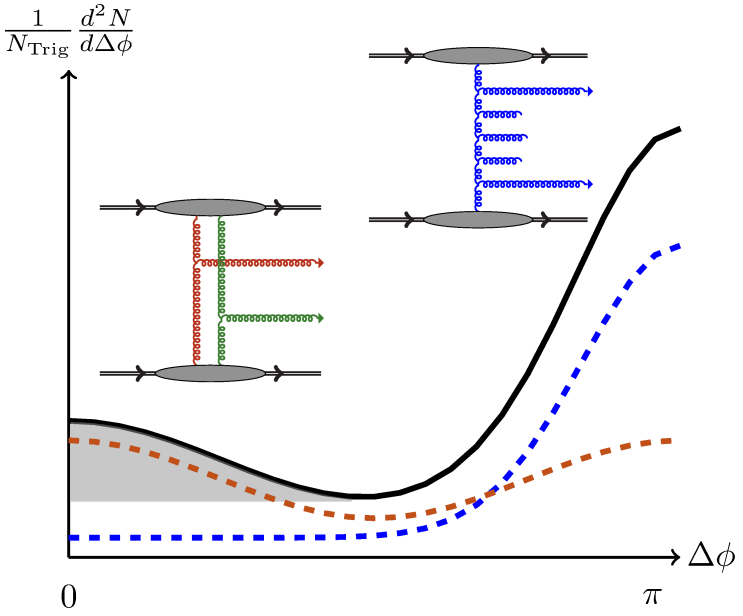

FIG. 1. The glasma graph on the left illustrates its schematic contribution to the double inclusive cross-section (dashed orange curve). On the right is the back-to-back graph and the shape of its yield (dashed blue curve). The gray blobs denote emissions all the way from beam rapidities to those of the triggered gluons. The solid black curve represents the sum of contributions from glasma and back-to-back graphs. The shaded region represents the Associated Yield (AY) calculated using the ZYAM procedure.

The other contribution, A_2 in Eq. (3) can be expressed as

$$\begin{aligned} A_2 = & \int_{\mathbf{k}_{1\perp}} \Phi_{A_1}(y_p,\mathbf{k}_{1\perp})\Phi_{A_1}(y_p,\mathbf{k}_{2\perp})\Phi_{A_2}(y_q,\mathbf{p}_T-\mathbf{k}_{1\perp})\Phi_{A_2}(y_q,\mathbf{q}_T+\mathbf{k}_{1\perp}) \\ & \times \frac{\left(\mathbf{k}_{1\perp}\cdot\mathbf{p}_T-\mathbf{k}_{1\perp}^2\right)\left(\mathbf{k}_{2\perp}\cdot\mathbf{p}_T-\mathbf{k}_{2\perp}^2\right)+\left(\mathbf{k}_{1\perp}\times\mathbf{p}_T\right)\left(\mathbf{k}_{2\perp}\times\mathbf{p}_T\right)}{\mathbf{k}_{1\perp}^2\left(\mathbf{p}_T-\mathbf{k}_{1\perp}\right)^2} \\ & \times \frac{\left(\mathbf{k}_{1\perp}\cdot\mathbf{q}_T-\mathbf{k}_{1\perp}^2\right)\left(\mathbf{k}_{2\perp}\cdot\mathbf{q}_T-\mathbf{k}_{2\perp}^2\right)+\left(\mathbf{k}_{1\perp}\times\mathbf{q}_T\right)\left(\mathbf{k}_{2\perp}\times\mathbf{q}_T\right)}{\mathbf{k}_{2\perp}^2\left(\mathbf{q}_T+\mathbf{k}_{1\perp}\right)^2} \end{aligned} \tag{4}$$

where $\mathbf{k}_{2\perp}\equiv\mathbf{p}_T-\mathbf{q}_T-\mathbf{k}_{1\perp}$.

The unintegrated gluon distribution (UGD) per unit transverse area Φ is a universal quantity determined by solving the Balitsky-Kovchegov (BK) equation [16, 17] as a function of the rapidity $y=\log(x_0/x)$. To avoid repetition, we refer the interested reader to Ref. [11] for identical details [18] of i) the derivation of Eqs. (1) and (3), ii) the expression for the single inclusive distribution, iii) solutions of the BK equation, iv) a discussion of the non-perturbative constant ζ in C_2 that represents the effect of soft multi-gluon interactions on the di-hadron spectrum.

We now turn to the double inclusive distribution from the back-to-back QCD graphs shown in Fig. 1. At high energies, for a pair of hadrons having a rapidity separation $\Delta y\gtrsim 1/\alpha_s$, a resummation of rapidity ordered multi-gluon emissions is necessary, corresponding to t-channel Pomeron exchange in the language of "Reggeon Field Theory" [19, 20]. Emissions between the two tagged partons lead to an angular decorrelation of the dihadron signal observed in the data. The observation of an angular decorrelation as a signal of pomeron exchange is complementary to looking for the growth in the dijet cross-section, as first proposed by Mueller and Navelet [21]. In this framework, the double inclusive multiplicity can be expressed as [22, 23]

$$\begin{aligned} \left.\frac{d^2N_{AB}}{d^2\mathbf{p}_T d^2\mathbf{q}_T dy_p dy_q}\right|_{\rm BFKL} &= \frac{32\,N_c\,\alpha_s(\mathbf{p}_T)\,\alpha_s(\mathbf{q}_T)}{(2\pi)^8\,C_F}\,\frac{S_\perp}{\mathbf{p}_T^2\mathbf{q}_T^2}K_{\rm BFKL} \\ &\times\int_{\mathbf{k}_{0\perp}}\int_{\mathbf{k}_{3\perp}}\Phi_A(x_1,\mathbf{k}_{0\perp})\Phi_B(x_2,\mathbf{k}_{3\perp})\,\mathcal{G}(\mathbf{k}_{0\perp}-\mathbf{p}_T,\mathbf{k}_{3\perp}+\mathbf{q}_T,y_p-y_q) \end{aligned} \tag{5}$$

where $\mathcal{G}$ is the BFKL Green's function

$$\mathcal{G}(\mathbf{q}_{a\perp},\mathbf{q}_{b\perp},\Delta y)=\frac{1}{(2\pi)^2}\frac{1}{(\mathbf{q}_{a\perp}^2\mathbf{q}_{b\perp}^2)^{1/2}}\sum_n e^{in\bar{\phi}}\int_{-\infty}^{+\infty}d\nu\;e^{\omega(\nu,n)\Delta y}e^{i\nu\ln\left(\mathbf{q}_{a\perp}^2/\mathbf{q}_{b\perp}^2\right)}\;. \tag{6}$$

The Φ's in the derivation of Eq. (5) are known as impact factors and, to next-to-leading-logarithmic (NLLx) accuracy in x, satisfy an integral equation where the kernel is the real part of the leading-logs in x (LLx) BFKL kernel [22, 24, 25]. Since the CMS di-hadron kinematics requires very significant evolution of the Φ's down from beam rapidities, well beyond the Mueller-Navelet regime, we will make the ansatz here that the Φ's are equivalent to the unintegrated gluon distributions in Eqs. (1) and (3) which are solutions of BK equation. Because of the very high parton densities in high multiplicity p+p events, it is not unreasonable to expect that BFKL evolution is modified to BK evolution. Because the BK equation includes multiple scattering effects on QCD evolution, one might expect multiple scattering effects on the BFKL Green function as well in these kinematics. Unfortunately, the technology to include these is unknown at present.

This systematic uncertainty from rescattering contributions to the BFKL Green function can be estimated as follows. A two gluon system produced in the BFKL framework, with large rapidity separation, corresponds to a large invariant mass. One anticipates that this system should be little affected by rescattering with the already shadowed gluons in the wave functions. This simple picture is borne out for heavy quark pair-production. In [26, 27], the rescattering (kt-factorization breaking) contributions to pair production were much less important (on the 10% level) when the invariant masses of the produced pair were greater than or equal to the saturation scale Q_S, while the shadowing corrections lead to qualitative changes at small x. Extending this estimate to the two gluon system, and taking into account the larger color factor, would give a 20% systematic uncertainty.

The role played by the BFKL Green's function can be demonstrated by "turning off" the gluon radiation between partons by taking the $\alpha_S \Delta y \to 0$ limit of the BFKL Green's function, obtaining the well known expression in Multi-Regge kinematics (MRK) [23, 28],

$$\left.\frac{d^2N_{AB}}{d^2\mathbf{p}_T d^2\mathbf{q}_T dy_p dy_q}\right|_{\rm MRK} = \frac{16\, N_c\, \alpha_s(\mathbf{p}_T)\, \alpha_s(\mathbf{q}_T)}{(2\pi)^8\, C_F}\, \frac{S_\perp}{\mathbf{p}_T^2 \mathbf{q}_T^2} \int_{\mathbf{k}_{1\perp}} \Phi_A(x_1, \mathbf{k}_{1\perp}) \Phi_B(x_2, \mathbf{k}_{2\perp})\,. \tag{7}$$

The universal BFKL Green's function in Eq. (6) resums leading logs in x, albeit with α_S chosen to run as the geometrical mean of the two momentum scales. NLLx expressions for this quantity are now known [22, 29] and are significantly more analytically cumbersome than Eq. (6). The moments $\mathcal{C}_m = \langle \cos m(\Delta\phi_{pq}) \rangle$ ($\langle \cdots \rangle$ denotes the $\frac{d^2N_{AB}}{d^2\mathbf{p}_T d^2\mathbf{q}_T dy_p dy_q}$ weighted average over ϕ_p,ϕ_q) have been computed numerically to estimate the relative LLx and NLLx contributions to the double inclusive distributions for relative rapidities $\Delta Y \geq 6$ [22, 30]. While the ratios $\mathcal{C}_{1,2}/\mathcal{C}_0$ are larger at NLLx by factors of 2-3 relative to LLx, this is largely because the $\Delta\phi_{pq}$ independent background $\mathcal{C}_0$ is significantly lower at NLLx relative to LLx. In contrast, the collimated contributions $\mathcal{C}_1$ and $\mathcal{C}_2$ at NLLx are larger than the LLx values by $\sim 10\%$ and 30% respectively. Thus the relatively small NLLx corrections to $\mathcal{C}_{1,2}$ suggest a LLx treatment may be adequate for studying collimated contributions. Further, because we include the effect of of running coupling both in the Φ's and $\mathcal{G}$–a piece of the NLLx contribution-the contributions neglected may be even smaller and comparable to other uncertainties such as choices of energy and renormalization scales.

We now turn to a quantitative comparison of the Glasma graphs (summing contributions from Eqs. (1), (3)) and back-to-back graphs (Eq. 5) and compute the associated yield per trigger [31] shown in the shaded region of Fig. (1). The detailed expressions for computing this yield implementing the ZYAM procedure are listed in [11]. The results for the CMS high multiplicity (denoted here as "central p+p") events [10] are shown in Fig. (2). The agreement with data is quite good; the results in the $2 \leq p_T^{\rm asc} \leq 3$ GeV and $3 \leq p_T^{\rm asc} \leq 4$ windows have not been presented previously. While the trends are reproduced, the data is slightly underestimated with increasing $p_T^{\rm trig}$ (albeit within experimental uncertainties). We note that in the absence of a Monte-Carlo generator, we are unable to require $N_{\rm trig} \geq 2$, as done for the data, in each transverse momentum bin.

Inclusion of the contribution from Eq. (3) lowers the K-factor from $K_{\rm Glasma} = 2.3$ required previously in [11] to $K_{\rm Glasma} = 1$. An important caveat is that we have taken the BFKL contribution on the near-side to be independent of $\Delta\phi_{pq}$ for $\Delta\phi_{pq} \leq \pi/2$ in Figs. (2) and (3). This is practically the case; however, a very small anti-collimation on the nearside, completely negligible relative to the awayside amplitude, can skew the nearside "ridge" signal completely because it is so small in comparison. BFKL predictions are not of this accuracy–we will therefore conjecture that a more precise treatment of its dynamics will give a $\Delta\phi_{pq}$ independent nearside contribution "within ridge accuracy".

These theoretical uncertainties can be resolved by comparisons to data of the associated per trigger yield in p+Pb collisions [32]. In Fig. (3), we show predictions for the nearside ridge for both minimum bias (left) and central (right) p+Pb collisions. All parameters are fixed to be the same for p+p and p+Pb. The only difference [33] is the value of the initial scale Q_0 in the running coupling BK evolution of Φ for Pb nuclei. The initial saturation scale (in the fundamental representation) is taken to be three times that of the min. bias proton value, $Q_0^2 = 0.504$ GeV^2, and denotes what is meant in our context by "minimum bias" for lead ions. A value six times larger, $Q_0^2 = 1.008$ GeV^2, is used for "central" ions. Recall that the min. bias and "central" p+p values were taken to be $Q_0^2 = 0.168$ GeV^2 and $Q_0^2 = 0.672$ GeV^2 respectively [34]. The key message from Fig. (3) is the prediction that there is a ridge in min. bias p+Pb collisions at $\sqrt{s} = 5$ TeV, albeit smaller than that in "central" p+p data. The ridge is larger in central p+Pb

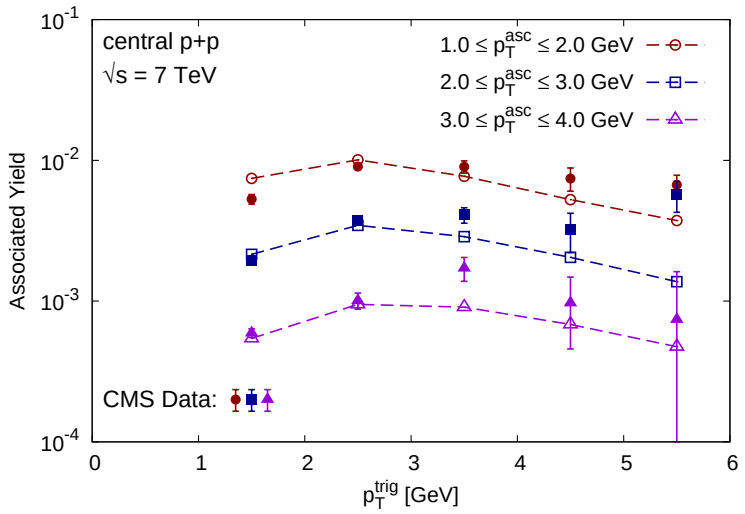

FIG. 2. The nearside yield per trigger as a function of $p_T^{\rm trig}$ in three different $p_T^{\rm asc}$ windows for high multiplicity p+p collisons. Filled symbols denote CMS data points extracted from the published $p_T^{\rm trig}$, $p_T^{\rm asc}$ di-hadron matrix [10]. Open symbols are our results, with dashed lines between points to guide the eye.

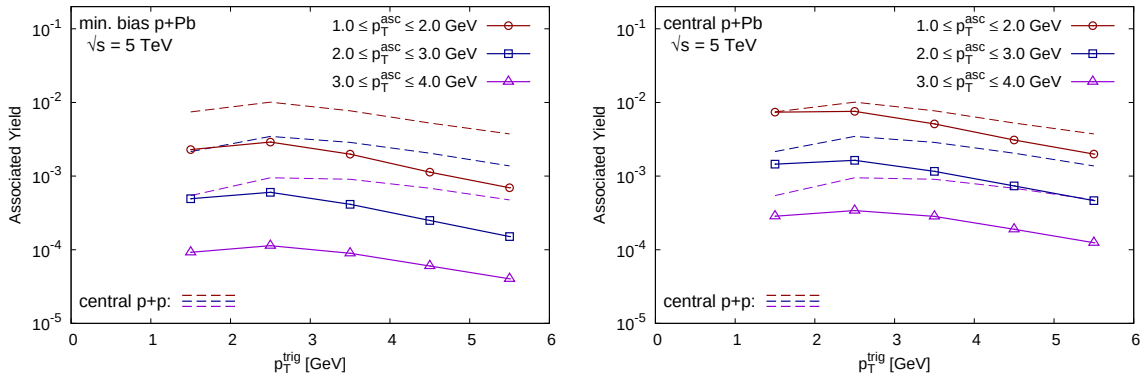

FIG. 3. The associated yield per trigger as a function of $p_T^{\rm trig}$ in min.bias p+Pb collisions at $\sqrt{s} = 5$ TeV (left) and central p+Pb collisions (right). Predictions are for the same $p_T^{\rm asc}$ windows as for high multiplicity p+p collisons, and results from the latter are presented for comparison as dashed lines.

collisions[35] slightly smaller than central p+p data.

In Fig. (4), we compare the "back-to-back" BFKL contribution in Eq. (5), which dominates the awayside $\Delta\phi_{pq}$ distribution to data in the $p_T^{\rm asc}$, $p_T^{\rm trig}$ matrix. This comparison also includes the awayside contribution from the Glasma graphs but, as discussed previously, this contribution is small. Because BFKL at the accuracy computed gives a "small" nearside anticollimation, this changes the Glasma K-factor from unity to $K = 2.3$. How this reweighting affects Fig. 2 is discussed in the appendix. The BFKL result gives good agreement with awayside data in the entire matrix in contrast to the result from the MRK expression in Eq. (7), as well as the result of a computation in quasi-multi-Regge-kinematics (QMRK) [23, 28]. In Fig. (5), we plot our prediction for the awayside di-hadron yield per unit $N_{\rm trig}$ in p+Pb collisions at $\sqrt{s} = 5$ TeV compared to the same in central p+p.

It will be interesting to extend our predictions for di-hadron spectra to di-jet production [36, 37] which has a larger rapidity acceptance at the LHC. Such tests of di-hadron spectra over the entire $\Delta\phi_{pq}$ range in p+p and p+Pb collisions have the potential to provide fundamental insights into the nature of QCD bremsstrahlung and gluon saturation at high energies.

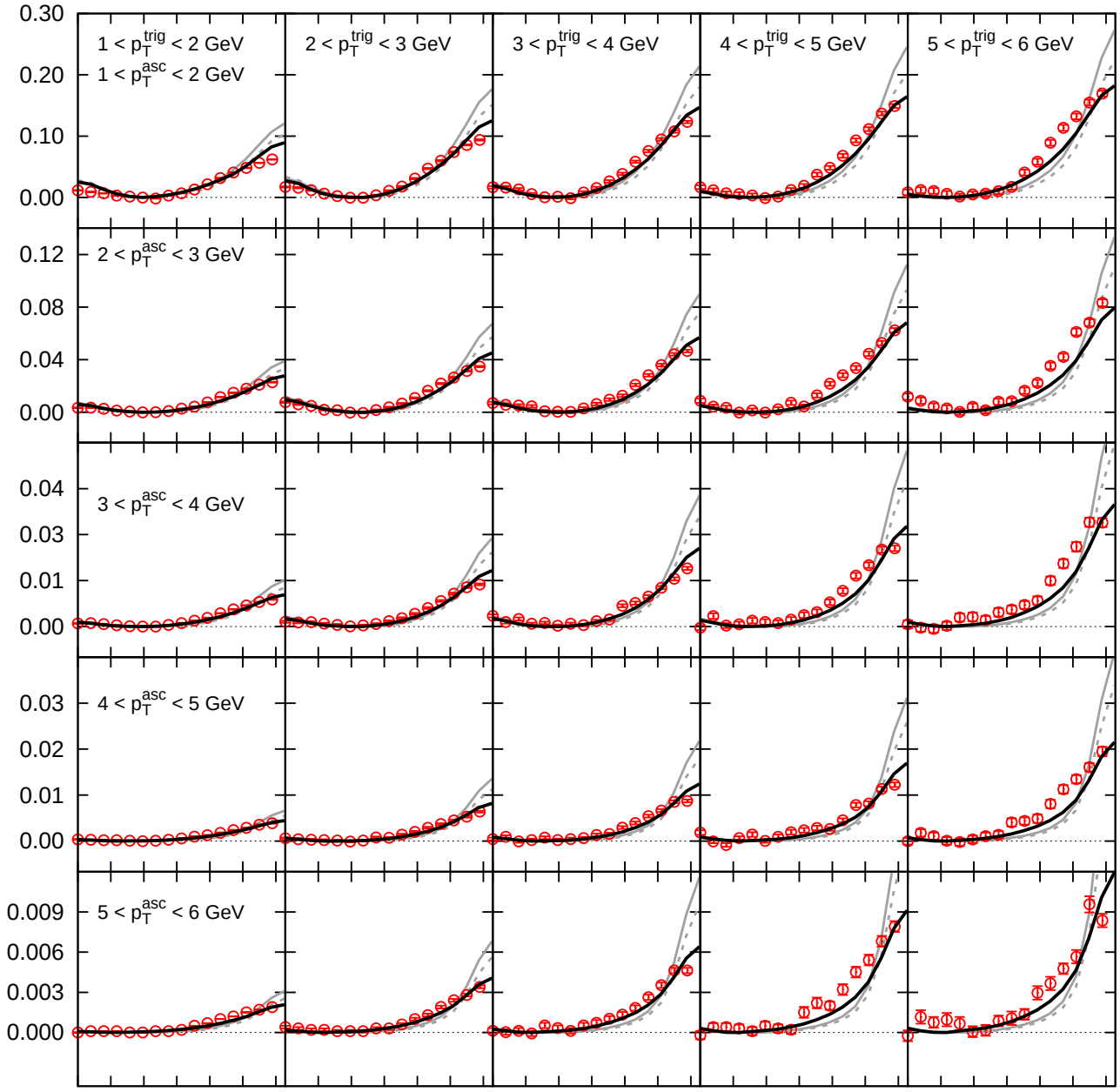

FIG. 4. CMS data after the removal of the underlying event in each bin via the ZYAM procedure. The solid curve is the BFKL result added to the Glasma result with K-factors of $K_{\rm BFKL} = 1.1$ and $K_{\rm Glasma} = 2.3$. The solid (dashed) gray curves show the result without BFKL evolution in the MRK (QMRK) framework.

Appendix A: Appendix A.

The magnitude of the near-side collimation as extracted via the ZYAM procedure is sensitive to the degree of near-side anti-collimation generated by the away-side BFKL graphs. Unfortunately, the systematic uncertainty of the near-side dynamics is much larger than the away-side contribution in the BFKL framework. In the BFKL framework the angular distribution always has a minimum at $\Delta\phi_{pq} = 0$. Clearly, this behavior is invalidated as one goes to small

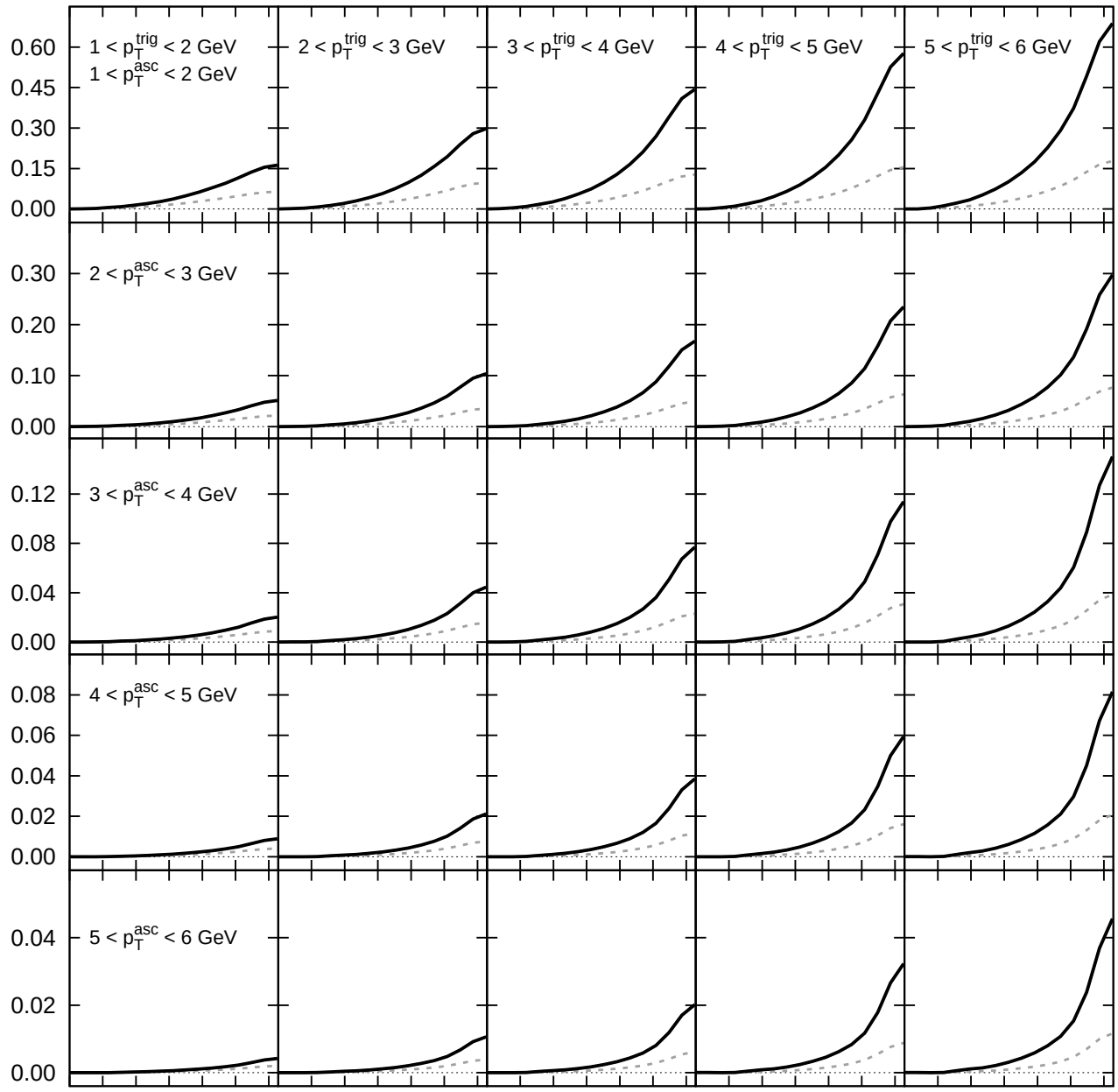

FIG. 5. BFKL prediction for the away-side yield in minimum bias p+Pb collisions at $\sqrt{s} = 5$ TeV. The gray curves show the corresponding results from central p+p. The underlying event has been subtracted from each bin.

rapidity separations having $|y_p - y_q| \leq 1$ where the recoiling near-side jet is clearly present in the angular distribution. It is not unlikely that the BFKL contribution has sizable systematic errors on the near-side at larger but still moderate rapidity separations, $|y_p - y_q| \sim 2$, which is the smallest separation included in the CMS acceptance.

Due to this larger near-side uncertainty, in evaluating the associated yield in Fig. 2 we have made the assumption that the background is flat for $\Delta\phi_{pq} \leq \pi/2$. In this case a K-factor, $K_{\rm Glasma} = 1$ was sufficient to explain the data.

The data in Fig 4 shows both the near and away-side contributions. Because of the BFKL uncertainty in the near-side we saw two possible ways to generate this plot. The first would be to use the analogous procedure of figure 3;

sum the Glasma contribution to a flat near-side background in the region $\Delta\phi_{pq} \leq \pi/2$ and use the BFKL contribution for $\Delta\phi_{pq} \geq \pi/2$. In this case a K-factor, $K_{\rm Glasma} = 1$, would have sufficed to explain the experimental data.

Instead we chose to add the Glasma contribution to the BFKL contribution computed at all angular separations, $0 \leq \Delta\phi_{pq} \leq \pi$. In this case the near-side collimation from the Glasma contribution has to compete against the artificial near-side anti-collimation produced by the BFKL graphs. An additional K-factor, $K_{\rm Glasma} = 2.3$, had to be used in order to account for this uncertainty in the near-side BFKL contribution.

One could ask how figure 2 would change if the near-side associated yield was extracted from figure 4 using the same ZYAM procedure used to produce figure 2. The resulting calculation is shown in Fig. 6.

The qualitative features of figure 2 remain the same; there are quantitative differences between the two calculations. The agreement is worse in the lowest associated p_T window than if the BFKL contribution is taken to be flat in the region $\Delta\phi_{pq} < \pi/2$, while for the higher associated p_T windows, the agreement is of comparable quality.

While this manuscript was under review, measurements of the two particle correlations in p+Pb collisions have become available [38]. In this case, the small correlations or anti-correlations from the BFKL graphs on the nearside are dwarfed by the Glasma graph contribution, and the K factors are of order unity[39]. Hence, our strong assumption of a $\Delta\phi_{pq}$ independent near-side is justified a posteriori–a positive interpretation is that by combining results of proton-proton and proton-lead collisions one can have a better handle on relative contributions of QCD graphs in high energy QCD.

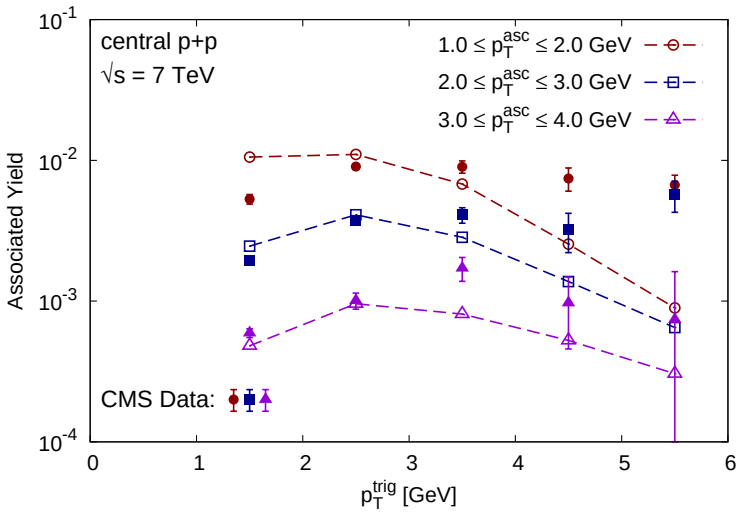

FIG. 6. The integrated associated nearside yield per trigger as a function of $p_T^{\rm trig}$ in three different $p_T^{\rm asc}$ windows for high multiplicity p+p collisons. Filled symbols denote CMS data points extracted from the published $p_T^{\rm trig}$, $p_T^{\rm asc}$ di-hadron matrix [10]. Open symbols are our results (including both Glasma and BFKL contributions to the nearside associated yield) with dashed lines between points to guide the eye.

ACKNOWLEDGMENTS

K.D. and R.V are supported by the US Department of Energy under DOE Contract Nos. DE-FG02-03ER41260 and DE-AC02-98CH10886 respectively. We would like to acknowledge useful conversations with Jochen Bartels, Dmitri Colferai, Francesco Hautmann and Samuel Wallon.

---

[1] I. Balitsky and L. Lipatov, Sov.J.Nucl.Phys. **28**, 822 (1978).
[2] E. Kuraev, L. Lipatov, and V. S. Fadin, Sov.Phys.JETP **45**, 199 (1977).
[3] Y. L. Dokshitzer, Sov.Phys.JETP **46**, 641 (1977).
[4] V. Gribov and L. Lipatov, Sov.J.Nucl.Phys. **15**, 438 (1972).
[5] G. Altarelli and G. Parisi, Nucl.Phys. **B126**, 298 (1977).
[6] L. Gribov, E. Levin, and M. Ryskin, Phys.Rept. **100**, 1 (1983).
[7] A. H. Mueller and J.-w. Qiu, Nucl.Phys. **B268**, 427 (1986).
[8] L. D. McLerran and R. Venugopalan, Phys.Rev. **D49** 2233 (1994), Phys.Rev. **D49** 3352 (1994).
[9] F. Gelis, E. Iancu, J. Jalilian-Marian, and R. Venugopalan, Ann.Rev.Nucl.Part.Sci. **60**, 463 (2010), arXiv:1002.0333 [hep-ph].
[10] V. Khachatryan *et al.* (CMS Collaboration), JHEP **1009**, 091 (2010), arXiv:1009.4122 [hep-ex].
[11] K. Dusling and R. Venugopalan, Phys.Rev.Lett. **108**, 262001 (2012), arXiv:1201.2658 [hep-ph].
[12] A. Dumitru, F. Gelis, L. McLerran, and R. Venugopalan, Nucl.Phys. **A810**, 91 (2008), arXiv:0804.3858 [hep-ph].
[13] K. Dusling, F. Gelis, T. Lappi, and R. Venugopalan, Nucl.Phys. **A836**, 159 (2010), arXiv:0911.2720 [hep-ph].
[14] A. Dumitru, K. Dusling, F. Gelis, J. Jalilian-Marian, T. Lappi, *et al.*, Phys.Lett. **B697**, 21 (2011), arXiv:1009.5295 [hep-ph].
[15] The delta function $\delta(\mathbf{p}_T \pm \mathbf{q}_T)$ in A_1 is broadened by multiple scattering as well as fragmentation effects the full treatment of which is beyond our scope. Here we smear the distribution to be $\delta(\phi_{pq}) \to \frac{1}{\sqrt{2\pi}\sigma} \exp\left(-\phi_{pq}^2/2\sigma^2\right)$, where $\Delta\phi_{pq} = \phi_p - \phi_q$ and $\sigma = 3$ GeV/$\mathbf{p}_T$ is a $\mathbf{p}_T$ dependent width on the order of the saturation scale. We stress that the associated yield–the integral over the near-side signal–is insensitive to details of this smearing.
[16] I. Balitsky, Nucl.Phys. **B463**, 99 (1996), arXiv:hep-ph/9509348 [hep-ph].
[17] Y. V. Kovchegov, Phys.Rev. **D60**, 034008 (1999), arXiv:hep-ph/9901281 [hep-ph].
[18] Variations relative to Ref. [11] are as follows: a) we take α_S to run as a function of $\mathbf{p}_T$ or $\mathbf{q}_T$ instead of the saturation scale Q_S. b) We use the NLO KPP parametrization [40] for gluon fragmentation to charged hadrons. c) The scale in the BK equation at the initial value $x = x_0$ is adjusted slightly to be $Q_0^2 = 0.168$ GeV^2 for min bias p+p collisions and $Q_0^2 = 0.672$ GeV^2 for central p+p collisions–we emphasize, as in Ref. [11], that this scale should not be confused with the much larger saturation scale Q_S.
[19] L. Lipatov, Nucl.Phys. **B452**, 369 (1995), arXiv:hep-ph/9502308 [hep-ph].
[20] V. Del Duca(1995), arXiv:hep-ph/9503226.
[21] A. H. Mueller and H. Navelet, Nucl.Phys. **B282**, 727 (1987).
[22] D. Colferai, F. Schwennsen, L. Szymanowski, and S. Wallon, JHEP **1012**, 026 (2010), arXiv:1002.1365 [hep-ph].
[23] V. S. Fadin, M. Kotsky, and L. Lipatov(1996), arXiv:hep-ph/9704267 [hep-ph].
[24] V. S. Fadin and A. D. Martin, Phys.Rev. **D60**, 114008 (1999), arXiv:hep-ph/9904505 [hep-ph].
[25] J. Bartels, D. Colferai, and G. Vacca, Eur.Phys.J. **C29**, 235 (2003), arXiv:hep-ph/0206290 [hep-ph].
[26] H. Fujii, F. Gelis, and R. Venugopalan, Nucl.Phys. **A780**, 146 (2006), arXiv:hep-ph/0603099 [hep-ph].
[27] H. Fujii, F. Gelis, and R. Venugopalan, Phys.Rev.Lett. **95**, 162002 (2005), arXiv:hep-ph/0504047 [hep-ph].
[28] A. Leonidov and D. Ostrovsky, Phys. Rev. **D62**, 094009 (2000), arXiv:hep-ph/9905496.
[29] J. R. Andersen and A. Sabio Vera, Nucl.Phys. **B679**, 345 (2004), arXiv:hep-ph/0309331 [hep-ph].
[30] F. Caporale, D. Y. Ivanov, B. Murdaca, and A. Papa(2012), arXiv:1209.6233 [hep-ph].
[31] The transverse overlap area in the collision $S_\perp$ cancels in this ratio. Another key feature of the ZYAM procedure is that $\Delta\phi_{pq}$-independent contributions, which are known to receive contributions from multiple sources in QCD [41–44], do not contribute.
[32] Both Glasma and BFKL graphs were considered previously in [45] to address forward-central di-hadron correlations in deuteron-gold collisions at RHIC. BFKL graphs were also discussed in the context of deuteron-gold collisions at RHIC in [46].
[33] These values for Q_0 for the proton and Lead are (imperfectly) constrained by fits to available p_T and rapidity distributions from RHIC and LHC for p+p and deuteron-gold collisions, and for the former from HERA e+p data as well. Once data for these "bulk" quantities are available for p+Pb collisions, (very) limited fine tuning of our results may be feasible.
[34] These initial values should not be confused with the saturation momentum, defined here as the peak of $\Phi(y, \mathbf{k}_T)$, at the much smaller values of $x\sqrt{s} = p_T e^{\pm y}$ probed in the di-hadron studies here, which span (in the adjoint representation), $Q_S^2\left(x \sim 10^{-4 \div 5}\right) \sim 1 - 5$ GeV^2 respectively for initial saturation scales used in this work.
[35] In this context, one should note that the proton is always treated as min. bias in what we have called "central" p+Pb; one should choose larger values for the initial saturation scale for very high multiplicity p+Pb collisions where rare "hot spot" configurations of the proton are selected.

[36] M. Deak, F. Hautmann, H. Jung, and K. Kutak(2010), arXiv:1012.6037 [hep-ph].
[37] K. Kutak and S. Sapeta(2012), arXiv:1205.5035 [hep-ph].
[38] S. Chatrchyan *et al.* (CMS Collaboration), Physics Letters B(2012), arXiv:1210.5482 [nucl-ex].
[39] K. Dusling and R. Venugopalan(2012), arXiv:1211.3701 [hep-ph].
[40] B. A. Kniehl, G. Kramer, and B. Potter, Nucl. Phys. **B582**, 514 (2000), arXiv:hep-ph/0010289.
[41] A. Dumitru and J. Jalilian-Marian, Phys.Rev. **D81**, 094015 (2010), arXiv:1001.4820 [hep-ph].
[42] A. Dumitru, J. Jalilian-Marian, and E. Petreska, Phys.Rev. **D84**, 014018 (2011), arXiv:1105.4155 [hep-ph].
[43] A. Kovner and M. Lublinsky, Phys.Rev. **D83**, 034017 (2011), arXiv:1012.3398 [hep-ph].
[44] A. Kovner and M. Lublinsky(2011), arXiv:1109.0347 [hep-ph].
[45] D. Kharzeev, E. Levin, and L. McLerran, Nucl.Phys. **A748**, 627 (2005), arXiv:hep-ph/0403271 [hep-ph].
[46] K. Tuchin, Nucl.Phys. **A846**, 83 (2010), arXiv:0912.5479 [hep-ph].